J Mater Sci (2007) 42:7294–7298
DOI 10.1007/s10853-007-1606-x

# Effect of ingredient on optical properties of Ag/Cu metal alloy nanoclusters in silica glass

**Y. H. Wang · C. Z. Jiang · F. Ren · Q. Q. Wang · D. J. Chen · D. J. Fu**

Received: 4 July 2006 / Accepted: 12 February 2007 / Published online: 10 May 2007


**Abstract** Formation of Ag-rich and Cu-rich Ag–Cu alloy nanoclusters in silica by Ag/Cu ion sequential implantation has been studied. The formation of alloy nanocluster has been evidenced by optical absorption spectra and transmission electron microscopy (TEM). Fast nonlinear refractive index and nonlinear absorption coefficient were measured at 790 nm of wavelength for Ag–Cu alloy nanocluster composites by the Z-scan technique. With different Ag/Cu ratio, linear absorption and nonlinear absorption are different in near infrared (NIR) region. It is suggested that by changing the ingredient percentage of metals in alloy, different optical nonlinearities could be selectively obtained.

## Introduction

Metal nanoclusters possess interesting linear and nonlinear optical properties. Recently, there has been an increasing interest in the third-order nonlinear susceptibility and the photorefractive effect of noble-metal clusters embedded in dielectric matrices [1–4]. The type and size of the embedded metal clusters, the dielectric constant, thermal conductivity and heat capacity of the dielectric matrices influenced third-order nonlinearities of the metal/dielectric composite materials. Amongst the nanoclusters studied by earlier researchers, nonlinear absorption and nonlinear refraction were found to be higher in copper and copper containing nanomaterials [2]. For silver, nonlinear refractive index $\gamma$ change from positive to negative upon clusters growth [5]. The most conspicuous manifestation of confinement in optical properties of metal nanocluster composite glasses (MNCGs) is the appearance of the surface plasmon resonance (SPR) that strongly enhances their linear and nonlinear responses around SPR wavelength [2, 3]. However, for optical applications it is important to have an enhanced nonlinearity of composite materials at the specific wavelength of practical using for optical signal propagation. Therefore, application aspects of the material should be most relevant. In this paper, we focused our interest on analysising the formation and contrasting the optical absorption properties of Ag–Cu alloy nanocluster composites in the time range of *fs* at the NIR wavelength of 790 nm.

## Experiment

Ag and Cu ions were implanted sequentially into silica glass at room temperature using a MEVVA source implanter. The samples were named AgCu1:1 and AgCu1:3, which means the ratios of dose for Ag and Cu ions were 1:1 and 1:3, respectively. The total doses of AgCu1:1 and AgCu1:3 were about $1 \times 10^{17}$ions/cm$^2$ and $2 \times 10^{17}$ions/cm$^2$ with the ion flux densities of Ag and Cu about 2 mA/cm$^2$. The acceleration voltages (43 kV for Ag and 30 kV for Cu) were chosen to get the same projected range for the implanted species. Optical absorption spectra were recorded at room temperature using a UV–VIS dual-beam spectrophotometer with wavelengths from 900 to 200 nm. Transmission electron microscopy (TEM) observations

Y. H. Wang · C. Z. Jiang (✉) · F. Ren · Q. Q. Wang · D. J. Chen · D. J. Fu
Key Laboratory of Acoustic and Photonic Materials and Devices of Ministry of Education, Department of Physics, Wuhan University, Wuhan 430072, China
e-mail: czjiang@whu.edu.cn

were carried out with a JEOL JEM 2010 (HT) microscope operated at 200 kV. Selected area electron diffraction (SAED), bright field (BF) and dark field (DF) imaging techniques were used to determine the crystal structure, size distribution, and shape of nanoclusters. The measurements of third-order susceptibility $\chi^{(3)}$ were carried out using the standard Z-scan method at 790 nm with an optical parametric amplifier (OPA) pumped by a self-mode-locked Ti:$Al_2O_3$ laser regenerative amplifier. We employed 150-fs laser pulses at 76 MHz repetition rate. The peak intensity of 8.8 GW/cm$^2$ was selected for the two samples.

## Result and discussion

Figure 1 shows the optical absorption spectra of Ag/Cu sequentially implanted samples. For comparison, the optical absorption spectra of Ag implanted sample with a dose of $1 \times 10^{17}$ ions/cm$^2$ at an energy of 90 keV and Cu implanted sample with a dose of $1 \times 10^{17}$ ions/cm$^2$ at energy of 60 keV are also shown in the figure. The SPR peak positions are 442 nm and 558 nm for the AgCu1:1 and AgCu1:3 samples, which lie in between that of pure Ag and Cu nanoclusters (about 400 and 570 nm, respectively). Therefore, it shows that intermetallic Ag–Cu alloy nanoclusters maybe have been formed instead of two separated Ag and Cu nanoclusters, which on the contrary would give rise to a double-peaked spectrum. For the AgCu1:3 sample, the peak position is 558 nm, near to that of Cu nanoclusters. With Cu increase in Ag/Cu alloy, the SPR peak band are red shifted significantly.

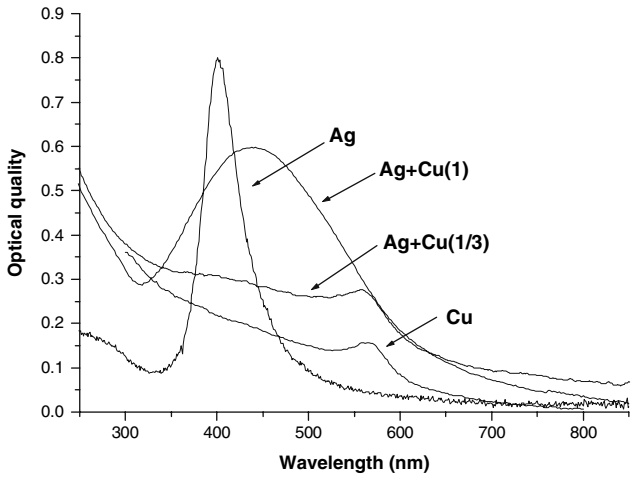


**Fig. 1** Optical density versus wavelength for Ag/Cu sequentially implanted sample with total doses of $1 \times 10^{17}$ ions/cm$^2$ (Ag/Cu = 1) and $2 \times 10^{17}$ ions/cm$^2$ (Ag/Cu = 1/3), Ag implanted sample with a dose of $1 \times 10^{17}$ ions/cm$^2$ and Cu implanted silica with a dose of $1 \times 10^{17}$ ions/cm$^2$

The TEM and SAED images of as-implanted AgCu1:1 and AgCu1:3 samples are shown in Figs. 2 and 3. Spherical clusters are formed during the implantation process. Selected area electron diffraction pattern for the Ag/Cu implanted samples are shown in Figs. 2(b) and Fig. 3(b), which can be indexed according to a single face-centered-cubic (fcc) phase with lattice constants $a_{AgCu1:1} = 0.396 \pm 0.002$ nm and $a_{AgCu1:3} = 0.369 \pm 0.002$ nm. They lie in between the lattice constants of Ag ($a_{Ag} = 0.408$ nm) and Cu ($a_{Cu} = 0.3608$ nm), indicating that Ag-rich and Cu-rich Ag–Cu alloy has been formed. The formation of alloy is related to the enhanced diffusion of Cu in small Ag clusters, just like adding Cu to Ag by the heat generated by the implantation that gives rise to high local temperatures [6, 7]. Molecular dynamic simulation on the displacement cascade has suggested that during the thermal spike of the cascade formation, the temperature in the cascade core can be extremely high and atoms inside the displacement cascade may achieve a 'liquid-like state' [8]. As the cooling rate of collision cascade is sufficiently high ($10^{14}$ K/s), Ag–Cu metastable alloy formed [9]. For the Ag–Cu alloy, there is no ordered phase, so these nanoclusters are an Ag–Cu solid solution.

The third-order nonlinear susceptibility can be written as $\chi^{(3)} = \chi_{\mathrm{Re}^{(3)}} + i\chi_{\mathrm{Im}^{(3)}}$, whose real part is related to the nonlinear refractive index coefficient $\gamma$, and the imaginary part is related to the nonlinear absorption coefficient $\beta$, and can be calculated as follows. Equation is valid only for $\alpha_0/2k \ll 1$, $\alpha_0$ is linear absorption coefficient, in our experiment $\alpha_0 = 1.5\ \mu\mathrm{m}^{-1}$ (for Ag/Cu1:1) and $\alpha_0 = 2.8\ \mu\mathrm{m}^{-1}$ (for Ag/Cu1:3), so it works.

$$\chi^{(3)}_{\mathrm{Re}} = 2\varepsilon_0 n_0^2 c\gamma \tag{1}$$

$$\chi^{(3)}_{\mathrm{Im}} = (\varepsilon_0 n_0^2 c^2 \beta)/\omega \tag{2}$$

$\beta$ and $\gamma$ can be determined by the Z-scan measurements with open- and close-aperture. When $|\beta I_0 L_{\mathrm{eff}}| \ll 1$, the theoretical relationship between $T$ and $z$ for the open-aperture configuration is given by [10].

$$T(z) = 1 - \frac{q_0}{2\sqrt{2}(1 + z^2/z_0^2)} \tag{3}$$

where $q_0 = \beta I_0 L_{\mathrm{eff}}$, $I_0$ is the intensity of the laser beam at the focus ($z = 0$), $L_{\mathrm{eff}}$ is the effective thickness of the sample. If the nonlinear medium exhibits nonlinear absorption, the closed-aperture data must be divided by the open-aperture data in order to obtain the purely refractive index. When $|\beta I_0 L_{\mathrm{eff}}| \le 1$, $|\beta/2k\gamma| \le 1$ and $|\Delta\phi_0| \ll 1$, the theoretical expression of the divided Z-scan transmittance can be written as [10]

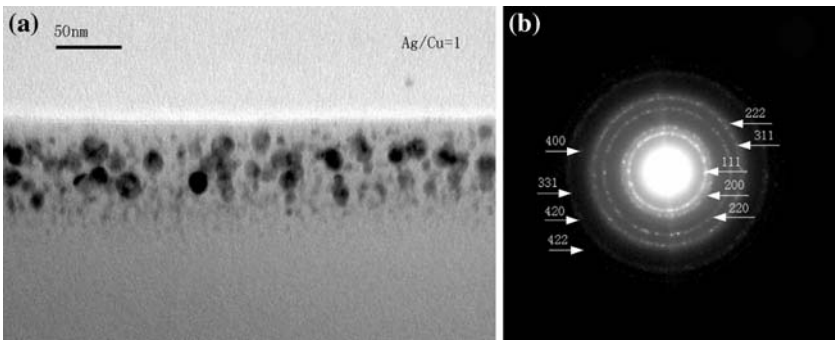


**Fig. 2** TEM bright-field (**a**) and SAED (**b**) images of the Ag/Cu 1:1 implanted silica

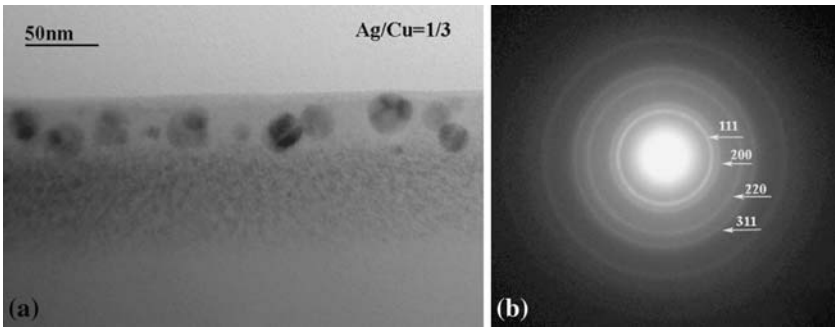


**Fig. 3** TEM bright-field (**a**) and SAED (**b**) images of the Ag/Cu 1:3 implanted silica

$$T(z) = 1 + \frac{4\Delta\Phi_0 x}{(x^2+9)(x^2+1)} \tag{4}$$

where $x = z/z_0$, $\Delta\Phi_0 = \frac{2\pi}{\lambda}\gamma I_0 L_{\text{eff}}$.

For the AgCu1:1 sample, Fig. 4 shows the normalized nonlinear transmittances versus the sample position measured with an open-aperture (a) and the value from the closed-aperture data divided by the open-aperture data (b). Nonlinear absorption and nonlinear refractive index of AgCu1:3 sample are shown in Fig. 5(a) and (b). As it can be seen from Figs. 4(a) and Fig. 5 (a), the open-aperture data are symmetric with respect to the focus and reveals positive nonlinear absorption coefficient which indicates the reverse saturable absorption (RSA). Obviously, with the increase of Cu ratio in Ag–Cu alloy, the RSA increased. The two samples exhibit different nonlinear refractive characters.

In our experiments, the minimum value of the beam radius waist $\omega_0$ is calculated to be about 4 μm. The solid curve in Figs. 4(a) and 5(a) are fitted by using Eq. (3) with the experiment parameters and the nonlinear absorption coefficients were obtained $\beta_{1:1} \approx 1.0 \times 10^{-6}$ cm/W and $\beta_{1:3} \approx 2.2 \times 10^{-6}$ cm/W. Fitting the Z-scan data of the closed-aperture with Eq. (4), we get values of $\gamma_{1:1} \approx -3.8 \times 10^{-12}$ cm$^2$/W and $\gamma_{1:3} \approx 4.3 \times 10^{-12}$ cm$^2$/W. Therefore, the absolute values of third-order nonlinear susceptibility for AgCu1:1 and AgCu1:3 samples are:

$$\begin{aligned}\chi^{(3)}_{1:1} &= [(\chi^{(3)}_{\text{Re}})^2 + (\chi^{(3)}_{\text{Im}})^2]^{1/2} \\ &= [(4.1\times10^{-9})^2 + (6.5\times10^{-9})^2]^{1/2} \\ &\approx 7.7\times10^{-9}\ \text{(esu)}.\end{aligned}$$

$$\begin{aligned}\chi^{(3)}_{1:3} &= [(\chi^{(3)}_{\text{Re}})^2 + (\chi^{(3)}_{\text{Im}})^2]^{1/2} \\ &= [(4.4\times10^{-9})^2 + (1.4\times10^{-8})^2]^{1/2} \\ &\approx 1.5\times10^{-8}\ \text{(esu)}.\end{aligned}$$

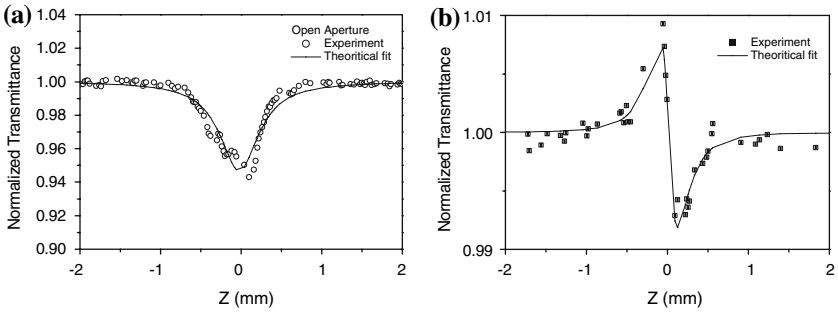


**Fig. 4** Normalized open-aperture (**a**) and the divided Z-scan result (**b**) of AgCu1:1 sample. Solid line: theoretical curve

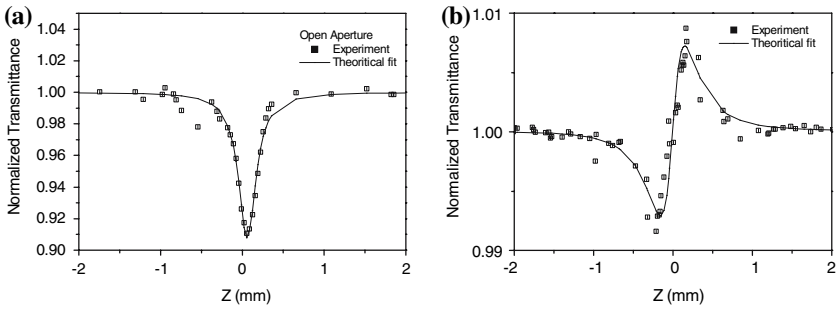


**Fig. 5** Normalized open-aperture (**a**) and the divided Z-scan result (**b**) of AgCu1:3 sample. Solid line: theoretical curve

Comparing $\chi^{(3)}_{\mathrm{Re}}$ with $\chi^{(3)}_{\mathrm{Im}}$ of two equations, nonlinear refractive $\chi^{(3)}_{\mathrm{Re}}$ has weak influence for $\chi^{(3)}$ than $\chi^{(3)}_{\mathrm{Im}}$ in two samples, the major causation for $\chi^{(3)}$ comes from nonlinear absorption. Local field enhancements in metal nanoclusters are known from electro-magnetic theory. In the quasi-static limit the local field inside a spherical particle, $E_{\mathrm{oc}}$, is related to the applied field $E_{\mathrm{o}}$ as [11]

$$E_{\mathrm{oc}} = \frac{3\varepsilon_{\mathrm{m}}(\omega)}{\varepsilon_{\mathrm{m}}(\omega) + 2\varepsilon_{\mathrm{d}}(\omega)} E_{\mathrm{o}} = f(\omega) E_{\mathrm{o}} \tag{5}$$

where $\varepsilon_{\mathrm{m}}$ is the complex dielectric response of the metal cluster, $\varepsilon_{\mathrm{d}}$ is the dielectric constant of the host material, and $f(\omega)$ is defined as the local-field factor. When $\varepsilon'_{\mathrm{m}}(\omega_{\mathrm{p}}) + 2\varepsilon_{\mathrm{d}} = 0$, the SPR occurs, the resonance is known as the collective oscillation of the conduction electrons, and the local field factor has maximal value. Ag and Cu have large real dielectric constant and small imaginary dielectric constant, when nanoclusters are irradiated by laser pulses, the SPR band gets excited, which leads to the dipole and higher order oscillations. These oscillations can couple with the applied electric field. Consequently, SPR frequency of excited atoms differs from that of unexcited atoms. The excited electrons are free carriers possessing a whole spectrum of energies. SPR band cannot further absorb in the original SPR band region. This leads to the ground-state plasmon band to bleach or reduce in intensity [12]. Bleaching of the absorption, which occurs in ultrafast timescale, is accompanied by the appearance of broad transient absorption on a wide side of the bleached region. A part of the excited electrons will be pumped to the even higher energy levels, causing excited-state absorption. The rest of the excited electrons have an energy higher than Fermi energy and get thermalized by dissipating excess energy through successive processes of electron-electron scattering, electron-surface scattering and electron-phonon scattering [13]. Exact timescales of all these processes may vary according to the type and environment of nanoclusters. Heat energy transferred to the surrounding medium. This excess thermal energy will increase the temperature of surrounding medium, which in turn influence the SPR. Full recovery of plasmon bleach is delayed and the transient absorption is occured till the thermalization of hot electrons is complete. The electron–electron scattering is very fast and occurs in femtosecond timescale. The broad transient absorption may consist of two components of Ag/Cu alloy and silica because of different timescales. During this transient period, aggregation may also result in the formation of large nanoclusters with very broad plasmon band. The RSA of the samples become more opaque on exposure to high photon fluxes due to the absorption from the excited state.

The use of high-repetition-rate lasers for Z-scan experiments also may trigger heating of the samples, giving rise to thermo-optical nonlinearities. In our experiment, comparing $\chi^{(3)}_{\mathrm{Re}}$ with $\chi^{(3)}_{\mathrm{Im}}$ in two samples, the nonlinear refractive $\chi^{(3)}_{\mathrm{Re}}$ weak influence for the $\chi^{(3)}$ in two samples, thus the thermal effect has minor influence for result in our experiment.

For Ag–Cu alloy nanoclusters in silica, the large volume fraction may also be a plummy factor for the result. Earlier reports on individual Cu and Ag nanoclusters of sizes in the range of 3–10 nm, measured with picosecond-pulsed lasers [14, 15] have shown a positive nonlinearity. However, in our case of Ag–Cu alloy nonoclusters, the cluster size varies from 15 to 40 nm, $L_{\mathrm{eff}}$ for AgCu1:1 and AgCu1:3 samples are 57 and 46 nm, respectively.

## Conclusion

In summary, Ag-rich and Cu-rich Ag–Cu alloy nanoclusters in silica have been formed by sequential ion implantation. The nonlinear optical properties were investigated by the Z-scan technique. The Ag/Cu metastable alloy nanoclusters in silica exhibits the peculiarity of linear and nonlinear absorption. With the increase of Cu content in alloy, linear absorption and nonlinear absorption increased in NIR region. We also think the high-volume fraction is one of factors leading in giant enhancement of the optical nonlinearities. With different Ag/Cu ratios, the alloy may lead to different optical nonlinearities. This is useful in fabrication of optical devices by control ingredient percentage of metals in alloy.

**Acknowledgements** This work was supported by the Natural Science Foundation of China (No. 10005005, 10375044, 10435060), the Key Project of Chinese Ministry of Education (No.104122) and Specialized Research Fund for the Doctoral Program of Higher Education (No. 20050486054).

## References

1. de Julián Fernández C, Tagliente MA, Mattei G, Sada C, Bello V, Maurizio C, Battaglin G, Sangregorio C, Gatteschi D, Tapfer L, Mazzoldi P (2004) Nucl Instr Meth B 216:245
2. Battaglin G, Cattaruzza E, De Marchi G, Gonella F, Mattei G, Maurizio C, Mazzoldi P, Parolin M, Sada C, Calliari I (2002) Nucl Instr Meth B 191:392
3. Cattaruzza E, Battaglin G, Calvelli P, Gonella F et al (2003) Compos Sci Tec 63:1203
4. Meldrum A, Boatner LA, White CW (2001) Nucl Instr Meth B 178:7
5. Ganeev RA, Ryasnyansky AI, Kamalov SR, Kodirov MK, Usmanov T (2001) J Phys D Appl Phys 34:1602
6. Mattel G (2002) Nucl Instr Meth B 191:232
7. Gonella F, Mattei G, Mazzoldi P, Sada C (1999) Appl Phys Lett 75:55
8. Wang LM, Wang SX, Ewing RC, Meldrum A, Birtcher RC, Provencio PN, Weber WJ, Matzke HJ (2000) Mater Sci Eng A 286:72
9. Poate JM, Borders JA, Cullis AG, Hirvonen JK (1977) Appl Phys Lett 30:365
10. Sheik-Bahae M, Said AA, Wei TH et al (1990) IEEE J Quantum Electron 26:760
11. Bloemer MJ, Haus JW, Ashley PR (1990) J Opt Soc Am B7:790
12. Kamat PV, Flumiani M, Hartland GV (1998) J Phys Chem B102:3123
13. Bigot JY, Halte V, Merle JC, Daunois A (2000) Chem Phys A 251:181
14. Hamanaka Y, Nakamura A, Omi S et al (1999) Appl Phys Lett 75:1712
15. Ballesteros JM, Sollids J, Serna R, Afonso CN (1999) Appl Phys Lett 74:2791